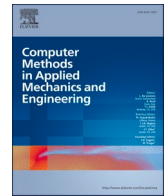




ELSEVIER

Contents lists available at ScienceDirect

Computer Methods in Applied Mechanics and Engineering

journal homepage: www.elsevier.com/locate/cma

Adaptive single-loop reweighted numerical integration for estimating response moment functions under hybrid aleatory and epistemic uncertainties

Jiaran Liu ^{a,b}, Marcos A. Valdebenito ^b, Dixiong Yang ^{a,*}, Matthias G.R. Faes ^{b,c,*}

^a State Key Laboratory of Structural Analysis, Optimization and CAE software for Industrial Equipment, Department of Engineering Mechanics, Dalian University of Technology, Dalian 116024, China

^b Chair for Reliability Engineering, TU Dortmund University, Dortmund 44227, Germany

^c International Joint Research Center for Engineering Reliability and Stochastic Mechanics, Tongji University, Shanghai 200092, China

ARTICLE INFO

Keywords:

Hybrid uncertainties
Response moment functions
Adaptive single-loop reweighted numerical integration
APEK point-selection strategy
Parallel computation

ABSTRACT

Efficient estimation of response moment functions under hybrid aleatory and epistemic uncertainties remains challenging because it requires multidimensional integration and repeated evaluations of complex system responses. This paper proposes an adaptive single-loop reweighted numerical integration (adaptive SLRNI) approach for evaluating the response mean and standard deviation functions, as well as their bounds, within the framework of the direct probability integral method. The original SLRNI approach relies on complex Voronoi partitioning and empirically specified numbers of representative points. To overcome these limitations, an adaptive probability-equalized k -nearest-neighbor (APEK) point-selection strategy is devised to generate uniformly distributed representative points with balanced probability weights. An adaptive batch-enrichment mechanism incrementally adds points according to a prescribed precision criterion, which eliminates empirical parameter selection and allows parallel computation. Moreover, the generalized probability density integral equations (PDIEs) are introduced to describe the probabilistic mapping between hybrid uncertain inputs and system responses. The response moment functions are derived from the PDIEs and then reformulated through a generalized reweighting scheme using a complete auxiliary density. By combining the APEK point-selection strategy with the single-loop reweighting scheme, the proposed adaptive SLRNI enables accurate computation of moment functions and their bounds without nested sampling. The approach is non-intrusive and applicable to nonlinear multiphysics coupled dynamic systems. Four examples, including a mathematical problem, a cantilever tube, a 120-bar truss and an offshore wind turbine tower, are presented to demonstrate the accuracy, efficiency, and versatility of the proposed approach.

1. Introduction

Uncertainties in engineering structural systems arise from various sources, including geometric parameters, material properties, and environmental loads. These uncertainties are commonly categorized into two types [1,2]: aleatory uncertainty, which results from

* Corresponding authors.

E-mail addresses: yangdx@dlut.edu.cn (D. Yang), matthias.faes@tu-dortmund.de (M.G.R. Faes).

<https://doi.org/10.1016/j.cma.2026.119001>

Received 15 December 2025; Received in revised form 27 March 2026; Accepted 13 April 2026

Available online 23 April 2026

0045-7825/© 2026 The Author(s). Published by Elsevier B.V. This is an open access article under the CC BY license (<http://creativecommons.org/licenses/by/4.0/>).

inherent randomness, and epistemic uncertainty, which stems from limited data or incomplete knowledge. In practice, these two types of uncertainty rarely occur in isolation and more often coexist and interact [3]. Therefore, rigorous quantification of both aleatory and epistemic uncertainties is essential for reliable performance assessment and safety evaluation of structural systems [4].

Several imprecise probability models have been developed to represent hybrid uncertainties, such as evidence theory [5–8], fuzzy possibility models [9–12], and probability boxes (p-boxes) [13–16]. Among these, p-boxes have attracted considerable attention because of their structural simplicity and their ability to explicitly distinguish between aleatory and epistemic uncertainties. In general, p-boxes are classified into distribution-free p-boxes [17] and parametric p-boxes [13]. The present study focuses on the parametric p-box representations. Under parametric p-boxes, the statistical moments of structural responses become functions of interval-valued distribution parameters rather than fixed quantities. For real-world engineering problems, closed-form expressions of these moment functions are often unavailable. Moreover, their numerical computation can be computationally intensive, as it requires multidimensional numerical integration even for a single realization of distribution parameters. Nevertheless, response moment functions play a fundamental role in structural uncertainty quantification because they characterize the probabilistic behavior of structural systems and provide essential information for reliability assessment and decision-making.

For analyzing response moments of systems under parametric p-boxes, existing methods can generally be divided into double-loop and single-loop approaches. Double-loop approaches include sampling-based nested methods, in which the outer loop performs sampling while the inner loop conducts response simulations. Representative approaches include the double-loop Monte Carlo simulation (DLMCS) [18], the interval Monte Carlo method [19] and the vertex-based DLMCS [20,21]. However, these methods can become computationally prohibitive for complex structural models. Another class of double-loop approaches consists of the optimization-integration nested methods, where interval parameters are treated as design variables in the outer loop and numerical integration is performed in the inner loop. Representative techniques include the optimized parameter sampling [20], the optimized univariate dimension-reduction method (OUDRM) [22] and the optimized sparse grid numerical integration method (OSGNI) [23,24]. Although more efficient than sampling-based nested methods, these approaches rely on gradient-based optimizers and may suffer from convergence to local optima. To mitigate this issue, global optimization techniques, such as genetic algorithms [25] and Bayesian global optimization [26], have been introduced. Nevertheless, these methods mainly provide the bounds of response statistics and cannot provide complete response moment functions.

To alleviate the computational burden associated with nested strategies, single-loop approaches have been proposed. Representative methods include the extended MCS [27], the non-intrusive imprecise stochastic simulation (NISS) [28] and the polynomial chaos expansion (PCE)-based methods [29,30]. The extended MCS and NISS eliminate nested simulations but still rely on repeated probabilistic sampling, which may remain computationally expensive for high-dimensional problems. PCE-based methods have been extended to parametric p-box propagation through augmented stochastic spaces or conditional surrogate constructions. Such dimensional augmentation leads to a rapid growth of polynomial basis terms as the combined uncertainty dimension increases, thereby giving rise to the curse of dimensionality. Recent advances in surrogate-based active learning methods, such as the non-intrusive imprecise probabilistic integration (NIPI) [31], the collaborative and adaptive Bayesian optimization (CABO) [32] and the parallel Bayesian quadrature optimization (PBQO) [33], have further improved computational efficiency through adaptive sampling strategies. Nevertheless, surrogate construction typically assumes a certain level of smoothness in the response surface, which may reduce accuracy for strongly nonlinear or non-smooth structural responses.

Most existing single-loop or optimization-integration nested approaches are primarily designed to compute the bounds of response statistics, rather than calculating the complete response moment functions over the epistemic parameter domain. Accordingly, the evaluation of complete response moment functions under parametric p-boxes remains computationally demanding, especially for complex finite element (FE) models and nonlinear dynamic structures with moderate to high levels of overall uncertainty. Therefore, developing accurate and efficient algorithms that avoid nested constructions and dimensional enlargement remains a crucial open challenge.

Recently, the direct probability integral method (DPIM) [34,35] has been proposed as a unified framework for stochastic uncertainty quantification, with several subsequent developments reported in [36–39]. Inspired by DPIM, a single-loop reweighted numerical integration (SLRNI) approach [40] was previously developed for reliability analysis under parametric p-boxes. Although it can be extended to moment evaluation, the original SLRNI employs a generalized F-discrepancy (GF)-based point-selection strategy [41] to generate representative points and their assigned probabilities for numerical integration. However, this procedure requires Voronoi partitioning and a large number of Monte Carlo samples for probability assignment, while the number of representative points must also be specified in advance.

To address these limitations, a novel adaptive probability-equalized k -nearest-neighbor (APEK) point-selection strategy is proposed. By integrating the suggested reweighting scheme with this point-selection strategy, an adaptive SLRNI approach is developed to evaluate the response mean and standard deviation functions under parametric p-boxes within a single-loop computational framework. The proposed approach enables the direct reconstruction of response moment functions over the epistemic parameter domain. The main contributions of this work are summarized as follows:

- (1) Generalized probability density integral equations (PDIEs) are formulated to characterize the probabilistic mapping between hybrid aleatory-epistemic uncertain inputs and structural responses. Based on these formulations, rigorous theoretical expressions for response moment functions under parametric p-boxes are derived.
- (2) By introducing a complete auxiliary density function, the moment functions are reformulated into a numerically tractable form. On this basis, a reweighting-based single-loop computational framework is established to evaluate the response mean and standard deviation functions without dimensional augmentation or nested simulation.

- (3) A novel APEK point-selection strategy is proposed to improve the efficiency and stability of numerical integration. The assigned probabilities are estimated using local k -nearest-neighbor volumes, and the representative point set is adaptively enriched according to a prescribed accuracy criterion.

Unlike surrogate-based approaches such as PCE constructed in augmented stochastic spaces, the proposed framework reformulates response moment functions through a reweighting mechanism in the original uncertainty space. This formulation avoids dimensional augmentation while preserving a strictly single-loop computational form.

The remainder of this paper is organized as follows. Section 2 formulates the problem considered in this study and introduces the generalized PDIEs for quantifying hybrid aleatory and epistemic uncertainties. Section 3 presents the theoretical basis and implementation procedure of the adaptive SLRNI approach. Section 4 presents several representative examples to validate the performance of the proposed approach. Section 5 provides concluding remarks and outlines directions for future research.

2. Preliminaries

This section presents a unified theoretical foundation based on the generalized PDIEs for hybrid uncertainty quantification. [Section 2.1](#) formulates the hybrid aleatory-epistemic uncertainty model, and [Section 2.2](#) derives the associated response moment functions via PDIEs.

2.1. Hybrid aleatory-epistemic uncertainty model

For a static structural system under parametric p-boxes, the response of interest Z is defined as:

$$Z = g(\mathbf{X}|\theta), \theta \in D_\theta, \quad (1)$$

where $\mathbf{X} = (X_1, X_2, \dots, X_n)$ is an n -dimensional input random vector whose components X_i are assumed to be mutually independent; $g(\cdot)$ denotes the structural response function that maps random vector \mathbf{X} to the response Z . Aleatory uncertainty is associated with the inherent randomness of \mathbf{X} , and the probability distribution type of each X_i is assumed to be known. Epistemic uncertainties arise from incomplete knowledge of the distribution parameters (e.g., the mean and standard deviation) of the input variables \mathbf{X} . Epistemic uncertainties are collected in an interval vector θ , whose admissible domain \mathcal{D}_θ is defined as:

$$\mathcal{D}_\theta = [\theta_1^L] \times \dots \times [\theta_m^L], \quad (2)$$

where each component $\theta_i^L = [\theta_i^L, \theta_i^U]$ is defined over an interval with lower and upper bounds θ_i^L and θ_i^U ; m is the number of interval parameters; here, the symbol ' \times ' denotes the Cartesian product. Thus, the joint probability density function (PDF) of \mathbf{X} conditional on a given θ is denoted by $p_{\mathbf{X}}(\mathbf{x}|\theta)$.

For a dynamic structural system under such parametric p-boxes, the dynamic response function can be expressed as:

$$Z(t) = g(\mathbf{X}|\theta, t), \theta \in D_\theta$$

where $Z(t)$ denotes the structural response at time t for a given realization of the input uncertainties. The extreme-value response within a given time interval $(0, T]$ is often of particular interest, since it significantly influences system performance and first-passage reliability. The extreme-value response Z_{ext} is defined as:

$$Z_{\text{ext}} = g_{\text{ext}}(\mathbf{X}|\theta) = \max_{t \in (0, T]} \{g(\mathbf{X}|\theta, t)\}, \theta \in D_\theta \quad (3)$$

where $g_{\text{ext}}(\cdot)$ represents the extreme-value operator that maps the dynamic response over the time interval $(0, T]$ to the maximum value Z_{ext} .

This study investigates the moment functions of the response of interest and the extreme-value response for static and dynamic structural systems, as defined in [Eqs. \(1\)](#) and [\(3\)](#), respectively. In the present formulation, the interval parameters are assumed to be mutually independent.

2.2. Formulation of response moment functions via generalized PDIE

Within the framework of the DPIM [[34,35](#)], PDIEs are established to characterize the propagation of pure random uncertainty. In [Ref. \[42\]](#), recent theoretical developments of PDIEs are presented via the probability conservation at the differential element and Dirac delta function.

In this section, the generalized PDIEs are formulated to describe the relationship between PDFs of hybrid uncertain inputs and PDFs of structural responses. Explicit expressions for response moment functions are subsequently derived based on the generalized PDIEs.

For a static structural system subjected to parametric p-boxes, the PDF $p_Z(z|\theta)$ of response at the given epistemic parameters θ can be expressed as:

$$p_Z(z|\theta) = \int_{\Omega_X} \delta[z - g(x)]p_X(x|\theta)dx, \tag{4}$$

where $\delta(\cdot)$ is the Dirac delta function; Ω_X denotes the admissible domain (support) of the input random variables.

The i -th raw moment function $m_i(\theta)$ of response Z is defined as:

$$m_i(\theta) = \mathbb{E}[g^i(x|\theta)] = \int_{\Omega_Z} z^i p_Z(z|\theta) dz. \tag{5}$$

Substituting Eq. (4) into Eq. (5) yields:

$$m_i(\theta) = \int_{\Omega_Z} \int_{\Omega_X} \delta[z - g(x)]z^i p_X(x|\theta) dx dz = \int_{\Omega_X} \left\{ \int_{\Omega_Z} \delta[z - g(x)]z^i dz \right\} p_X(x|\theta) dx. \tag{6}$$

By utilizing the sifting property of the Dirac delta function, $m_i(\theta)$ can be rewritten as:

$$m_i(\theta) = \int_{\Omega_X} g^i(x) p_X(x|\theta) dx. \tag{7}$$

From Eq. (7), the response mean and variance functions can be obtained as:

$$\mu(\theta) = m_1(\theta) = \int_{\Omega_X} g(x) p_X(x|\theta) dx, \tag{8}$$

and

$$\sigma^2(\theta) = m_2(\theta) - (m_1(\theta))^2 = \int_{\Omega_X} g^2(x) p_X(x|\theta) dx - \mu(\theta)^2. \tag{9}$$

For a dynamic structural system under hybrid uncertainties, the generalized PDIE can be formulated as:

$$p_Z(z|\theta, t) = \int_{\Omega_X} \delta[z(t) - g(x, t)] p_X(x|\theta) dx, \tag{10}$$

where $p_Z(z|\theta, t)$ denotes the instantaneous PDF of dynamic response at θ .

The generalized PDIEs in Eqs. (4) and (10) characterize the propagation of the PDFs of the input variables to the output response PDFs for static and dynamic structural systems, respectively.

In this study, the extreme-value response for dynamic structural systems is of particular interest. Its PDF can be expressed as:

$$p_{Z_{\text{ext}}}(z_{\text{ext}}|\theta) = \int_{\Omega_X} \delta[z_{\text{ext}} - g_{\text{ext}}(x)] p_X(x|\theta) dx. \tag{11}$$

The mean and variance functions of the extreme-value response are obtained from Eq. (11), yielding:

$$\mu_{\text{ext}}(\theta) = \int_{\Omega_X} g_{\text{ext}}(x) p_X(x|\theta) dx, \tag{12}$$

and

$$\sigma_{\text{ext}}^2(\theta) = \int_{\Omega_X} g_{\text{ext}}^2(x) p_X(x|\theta) dx - \mu_{\text{ext}}(\theta)^2. \tag{13}$$

The lower and upper bounds of the moment functions are determined through the following optimization problems.

Bounds on the mean:

$$\begin{aligned} \mu^L &= \min_{\theta \in \mathcal{D}_\theta} \mu(\theta), \mu_{\text{ext}}^L = \min_{\theta \in \mathcal{D}_\theta} \mu_{\text{ext}}(\theta) \\ \mu^U &= \max_{\theta \in \mathcal{D}_\theta} \mu(\theta), \mu_{\text{ext}}^U = \max_{\theta \in \mathcal{D}_\theta} \mu_{\text{ext}}(\theta) \end{aligned}, \tag{14}$$

Bounds on the standard deviation:

$$\begin{aligned} \sigma^L &= \min_{\theta \in \mathcal{D}_\theta} \sigma(\theta), \sigma_{\text{ext}}^L = \min_{\theta \in \mathcal{D}_\theta} \sigma_{\text{ext}}(\theta) \\ \sigma^U &= \max_{\theta \in \mathcal{D}_\theta} \sigma(\theta), \sigma_{\text{ext}}^U = \max_{\theta \in \mathcal{D}_\theta} \sigma_{\text{ext}}(\theta) \end{aligned} \tag{15}$$

Once the response moment functions are obtained, their bounds can be evaluated through optimization over the epistemic parameter domain. However, direct evaluation of these moment functions is computationally demanding, as it involves repeated response simulations and high-dimensional numerical integration. The present work aims to estimate response moment functions and their bounds through an adaptive single-loop reweighted computational framework.

3. The proposed adaptive SLRNI approach

Section 3.1 outlines the proposed SLRNI framework. Section 3.2 reformulates the response moment functions using an auxiliary density. Section 3.3 introduces the adaptive point-selection strategy and its integration with the reweighting scheme. Section 3.4 summarizes the implementation procedure.

3.1. Overview of the adaptive SLRNI

The basic response moment formulas Eqs. (8)-(13) involve multidimensional integrals that couple random variables and interval parameters. Direct evaluation is computationally demanding, especially for complex structural models. To address this difficulty, a complete auxiliary density is first introduced to reformulate moment functions into the reweighted integral forms. The proposed approach combines the reweighted formulations with an adaptive probability-equalized point-selection strategy to evaluate the response mean and standard deviation functions. Once the moment functions are obtained, their bounds are determined through optimization over the epistemic parameter space without additional model evaluations.

3.2. Auxiliary density-based response moment functions

Following the idea introduced in [40], a complete auxiliary density function is adopted to reformulate the response moment functions.

For a static structural system, the response mean function in Eq. (8) can be reformulated as:

$$\mu(\theta) = \int_{\Omega_x} \frac{g(\mathbf{x})p_x(\mathbf{x}|\theta)}{\phi(\mathbf{x})} \phi(\mathbf{x})d\mathbf{x}, \tag{16}$$

where $\phi(\mathbf{x})$ denotes the complete auxiliary density [40], which is defined as:

$$\phi(\mathbf{x}) = \frac{1}{\lambda} \int_{\mathcal{D}_\theta} p(\mathbf{x}|\theta)d\theta,$$

where λ is a normalization constant that ensures $\phi(\mathbf{x})$ is a valid PDF satisfying $\phi(\mathbf{x}) > 0$ for $\mathbf{x} \in \Omega_x$ and $\int_{\Omega_x} \phi(\mathbf{x})d\mathbf{x} = 1$. Here, $\phi(\mathbf{x})$ represents a normalized PDF obtained by integrating the conditional PDF $p_x(\mathbf{x}|\theta)$ over the interval parameter space. The auxiliary density shares the same support as the target distribution and remains strictly positive wherever the target density is nonzero. For numerical robustness, a small positive lower bound is imposed during the evaluation of the auxiliary density.

Similarly, the response variance function Eq. (9) can be rewritten as:

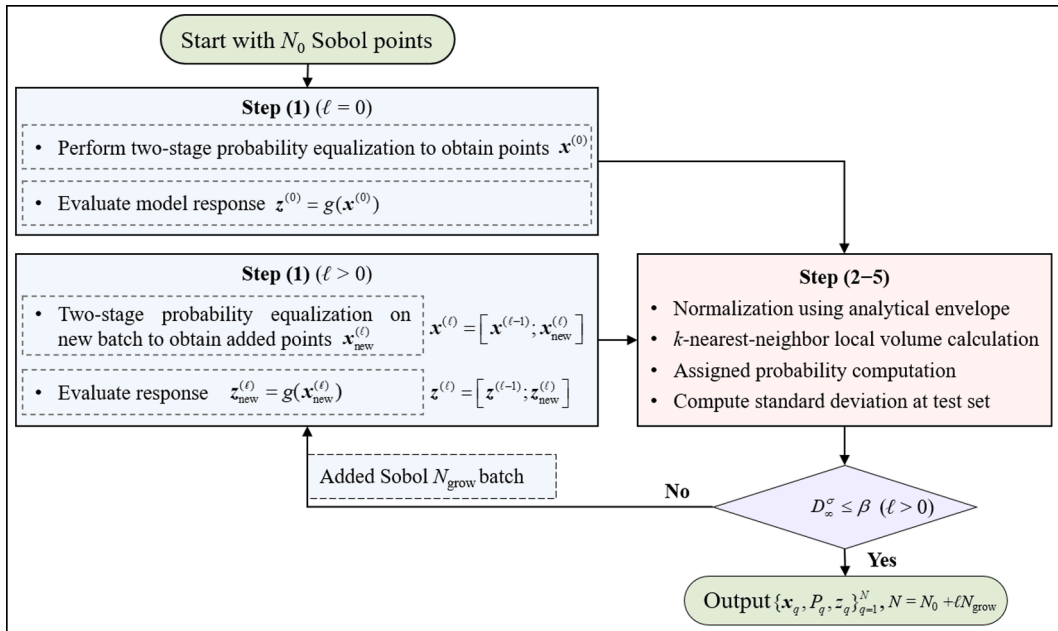


Fig. 1. Specific procedure of the proposed adaptive point-selection strategy.

$$\sigma^2(\theta) = \int_{\Omega_x} \frac{g(\mathbf{x})^2 p_X(\mathbf{x}|\theta)}{\phi(\mathbf{x})} \phi(\mathbf{x}) d\mathbf{x} - \left[\int_{\Omega_x} \frac{g(\mathbf{x}) p_X(\mathbf{x}|\theta)}{\phi(\mathbf{x})} \phi(\mathbf{x}) d\mathbf{x} \right]^2. \quad (17)$$

For a dynamic structural system, the response mean and variance functions become:

$$\mu_{\text{ext}}(\theta) = \int_{\Omega_x} \frac{g_{\text{ext}}(\mathbf{x}) p_X(\mathbf{x}|\theta)}{\phi(\mathbf{x})} \phi(\mathbf{x}) d\mathbf{x}, \quad (18)$$

and

$$\sigma_{\text{ext}}^2(\theta) = \int_{\Omega_x} \frac{g_{\text{ext}}(\mathbf{x})^2 p_X(\mathbf{x}|\theta)}{\phi(\mathbf{x})} \phi(\mathbf{x}) d\mathbf{x} - \left[\int_{\Omega_x} \frac{g_{\text{ext}}(\mathbf{x}) p_X(\mathbf{x}|\theta)}{\phi(\mathbf{x})} \phi(\mathbf{x}) d\mathbf{x} \right]^2. \quad (19)$$

These reformulated expressions form the basis for the adaptive numerical integration procedure developed in the following section. For simplicity, the model response is uniformly denoted by z , representing either the static response or the extreme-value response of dynamic systems.

3.3. APEK point-selection strategy

The APEK point-selection strategy is developed to generate representative points and their assigned probabilities for numerical integration of response moments in the reweighted computation described in Section 3.4. The key idea is to discretize the probability space induced by the auxiliary density using statistically representative samples. The procedure starts from an initial Sobol point set and iteratively enriches the representative points until convergence is achieved. The overall procedure consists of the following five steps, which are illustrated in Fig. 1.

Step (1) Probability equalization under auxiliary density.

Start. The strategy begins with an initial Sobol sample set $U^{(0)} = \{u_i\}_{i=1}^{N_0} \subset [0, 1]^n$ of size N_0 at iteration $\ell = 0$. Sobol sequences are used because of their low-discrepancy and space-filling properties. A two-stage probability equalization procedure is then performed to obtain the uniformly distributed representative points. First, each dimension u_j is mapped to the physical space by the inverse cumulative distribution function (CDF) Φ_j^{-1} of the auxiliary density:

$$\bar{x}_j = \Phi_j^{-1}(u_j) \quad j = 1, 2, \dots, n,$$

where the superscript ‘1’ denotes the first transformation and the superscript ‘0’ corresponds to the current iteration index $\ell = 0$. Rank-based probability equalization is subsequently applied:

$$\bar{u}_j = (\text{rank}(\bar{x}_j) - 0.5) / N_0.$$

Next, \bar{u}_j is mapped again with the inverse CDF Φ_j^{-1} :

$$x_j^{(0)} = \Phi_j^{-1}(\bar{u}_j)$$

to obtain the initial probability-equalized representative points $x^{(0)}$. Structural responses $z^{(0)} = g(x^{(0)})$ (responses of interest or extreme-value responses) are evaluated at these points.

3.3.1. Adaptive enrichment

At each iteration ℓ ($\ell = 1, 2, \dots$), the representative point set is enriched by appending a Sobol batch of size $N_{\text{grow}} \cdot U_{\text{new}}^{(\ell)} = \{u_i^{(\ell)}\}_{i=1}^{N_{\text{grow}}} \subset [0, 1]^n$. Only the newly added batch undergoes the two-stage probability equalization to produce the additional representative points $x_{\text{new}}^{(\ell)}$ and their model response evaluations $z_{\text{new}}^{(\ell)} = g(x_{\text{new}}^{(\ell)})$. The representative points and corresponding response evaluations are then updated through row-wise concatenation:

$$x^{(\ell)} = [x^{(\ell-1)}; x_{\text{new}}^{(\ell)}], z^{(\ell)} = [z^{(\ell-1)}; z_{\text{new}}^{(\ell)}]$$

Because enrichment is performed in batches, structural response evaluations can be estimated in parallel, which further improves the computational efficiency of the proposed method.

Steps (2)–(5) are then applied to the updated representative point set $x^{(\ell)}$. In these steps, the points contained in the set $x^{(\ell)}$ are swept using index q , $q = 1, 2, \dots, N_\ell, N_\ell = N_0 + \ell N_{\text{grow}}$ denotes the total number of representative points at iteration ℓ .

Step (2) Normalization using analytical envelope. The representative point set is normalized into the unit interval: $\tilde{x}_{qj} = (x_{qj} - a_j) / (b_j - a_j) \in [0, 1]^n$, so that all coordinates lie on a consistent metric scale. This ensures that subsequent k -nearest-neighbor local volume computations are well-conditioned.

The analytical envelope $[a_j, b_j]$ is constructed for geometric comparability across dimensions and to handle boundary effects. Three typical cases are considered:

- (i) precise distributions with known finite bound (such as a precise uniform): $[a_j, b_j] = [A_j, B_j]$;
- (ii) precise unbounded distributions characterized by mean and standard deviation (like precise normal): $[a_j, b_j] = [\mu_j - K\sigma_j, \mu_j + K\sigma_j]$; K is the envelope multiplier parameter, and is chosen between 6 and 8 (integer values).
- (iii) imprecise distributions with interval-valued parameters or strictly positive support (like imprecise lognormal/gamma): $[a_j, b_j] = [\max\{0, \mu_j^L - K\sigma_j^U\}, \mu_j^U + K\sigma_j^U]$.

Step (3) k -nearest-neighbor local volume calculation. To determine the local region represented by each representative point \mathbf{x}_q , the k -nearest-neighbor radius r_q is computed under the Chebyshev (L_∞) metric, inspired by standard k -nearest-neighbor density estimation techniques [43,44]. The metric L_∞ is adopted because it matches the hyper-rectangular epistemic domain and enables stable axis-aligned neighborhood construction. For each point $\tilde{\mathbf{x}}_q \in [0, 1]^n$, r_q is defined as the distance to its k -th nearest neighbor $\tilde{\mathbf{x}}_{(k)}$ under the L_∞ metric:

$$r_q = \|\tilde{\mathbf{x}}_q - \tilde{\mathbf{x}}_{(k)}\|_\infty. \tag{20}$$

Specifically, the distance of each $\tilde{\mathbf{x}}_q$ to every other point is evaluated and sorted, and the k -th smallest distance is taken as r_q . The value of r_q differs from point to point because it adapts automatically to the local point density. This means that dense regions yield smaller radii and sparse regions yield larger ones. A small value of $k \in \{6, 7, 8\}$ is adopted in accordance with empirical guidelines for k -nearest-neighbor density estimation [43,44], which helps control estimator variance in higher dimensions.

The radius r_q defines a hypercube neighborhood centered at $\tilde{\mathbf{x}}_q$ whose volume is given by:

$$V_q = \prod_{j=1}^n \max(0, \min(\tilde{x}_{qj} + r_q, 1) - \max(\tilde{x}_{qj} - r_q, 0)). \tag{21}$$

Although neighborhood-based estimators can be sensitive to dimensionality, the probability-equalized representative points exhibit approximately uniform distributions that reduce the effective intrinsic dimensionality. In practice, the method remains robust for moderate dimensions (approximately up to 15 uncertain variables) in hybrid uncertainty problems.

Step (4) Assigned probabilities computation. Each representative point \mathbf{x}_q receives a deterministic weight proportional to its local volume. The weight is then normalized to produce the assigned probabilities P_q :

$$P_q = \tilde{P}_q / \sum_k \tilde{P}_k, \tilde{P}_q = V_q \phi(\tilde{\mathbf{x}}_q). \tag{22}$$

where $\phi(\tilde{\mathbf{x}}_q)$ is the auxiliary joint density at each point $\tilde{\mathbf{x}}_q \in [0, 1]^n$. Hence, the assigned probability P_q reflects the local occupied k -nearest-neighbor volume at \mathbf{x}_q .

Step (5) Standard deviation computation at the test set

Selecting a batch of fixed Sobol points $\Theta^\star = \{\Theta_k\}_{k=1}^M, \Theta^\star \in D_\theta$ as the test point set, the standard deviation $\hat{\sigma}^{(\ell)}$ at Θ^\star is calculated through Eq. (26):

$$\hat{\sigma}^{(\ell)} = \sqrt{\sum_q w_q(\Theta_k) (z_q - \hat{\mu}^{(\ell)})^2}, \hat{\mu}^{(\ell)} = \sum_q w_q(\Theta_k) z_q \tag{23}$$

which is used in the stopping criterion. After the first enrichment iteration, the algorithm evaluates the stopping criterion to determine whether further enrichment is required.

3.3.2. Stopping criterion

The relative change of standard deviation between two successive iterations is estimated:

$$D_\infty^\sigma = \max_{1 \leq k \leq M} \frac{|\hat{\sigma}^{(\ell)} - \hat{\sigma}^{(\ell-1)}|}{|\hat{\sigma}^{(\ell-1)}|}, (L_\infty \text{ norm}) \tag{24}$$

The iterative enrichment process terminates when:

$$D_{\infty}^{\sigma} \leq \beta, \tag{25}$$

where β ($\beta \leq 0.02$) is the given threshold. Once this condition is satisfied, the algorithm terminates and outputs: $\{x_q, P_q, z_q\}_{q=1}^N$, where $N = N_0 + \ell N_{\text{grow}}$. Otherwise, the procedure returns to step (1) for further enrichment. The maximum threshold value of 0.02 is selected to balance accuracy and computational efficiency. Smaller values of β improve accuracy but require more representative points and more computations, while larger values ($\beta > 0.02$) reduce computation time but may slightly decrease accuracy. Numerical validation indicates that the method remains stable within this range.

The convergence criterion is evaluated on a fixed Sobol set Θ^* to ensure consistent low-discrepancy coverage of the epistemic parameter space. Since the response moments are monitored over the entire interval domain, the criterion reflects global functional convergence rather than local pointwise errors.

Remark 1. Four types of relative changes of response moments are examined on the Sobol test set:

$$D_1^{\mu} = \frac{1}{M} \sum_{k=1}^M \frac{|\hat{\mu}^{(\ell)} - \hat{\mu}^{(\ell-1)}|}{|\hat{\mu}^{(\ell-1)}|}, D_1^{\sigma} = \frac{1}{M} \sum_{k=1}^M \frac{|\hat{\sigma}^{(\ell)} - \hat{\sigma}^{(\ell-1)}|}{|\hat{\sigma}^{(\ell-1)}|}, \text{ (L}_1\text{ norm)}$$

$$D_{\infty}^{\mu} = \max_{1 \leq k \leq M} \frac{|\hat{\mu}^{(\ell)} - \hat{\mu}^{(\ell-1)}|}{|\hat{\mu}^{(\ell-1)}|}, D_{\infty}^{\sigma} = \max_{1 \leq k \leq M} \frac{|\hat{\sigma}^{(\ell)} - \hat{\sigma}^{(\ell-1)}|}{|\hat{\sigma}^{(\ell-1)}|}. \text{ (L}_{\infty}\text{ norm)}$$

The evolutions of these quantities with respect to the number of representative points are illustrated in Fig. 2 (Example 1 in Section 4). The results show that the convergence behavior is primarily governed by the relative change of the standard deviation D_{∞}^{σ} , which is selected as the stopping indicator.

Remark 2. To assess the quality of representative point generation and probability assignment, the results of the APEK point-selection strategy are illustrated in Fig. 3. Fig. 3(a) shows that the representative points are uniformly distributed over the support domain without noticeable clustering or boundary bias. The Gini index $= 1 - \sum_{i=1}^N P_q^2$ is employed to measure the evenness of the assigned probabilities [45]. A value close to zero indicates a more balanced probability distribution. As shown in Fig. 3(b), Gini index = 0.214 confirms a well-balanced probability assignment. The cumulative probability mass of the largest 1% and 5% assigned probabilities are 2.1% and 9.0%, respectively. These small values indicate that no small subset of representative points dominates the probability mass, which ensures numerical stability. Overall, these diagnostics demonstrate that the proposed APEK strategy generates a well-conditioned representative set suitable for accurate reweighted numerical integration.

3.4. Evaluation of response moment functions and their bounds

(1) Response moment function

Given the representative points x_q and weights P_q obtained from APEK point-selection strategy and the response evaluations z_q , the response moment functions at any interval parameter θ are computed via single-loop reweighted estimation based on Eqs. (16)–(19). The estimated mean and standard deviation functions of response are calculated by:

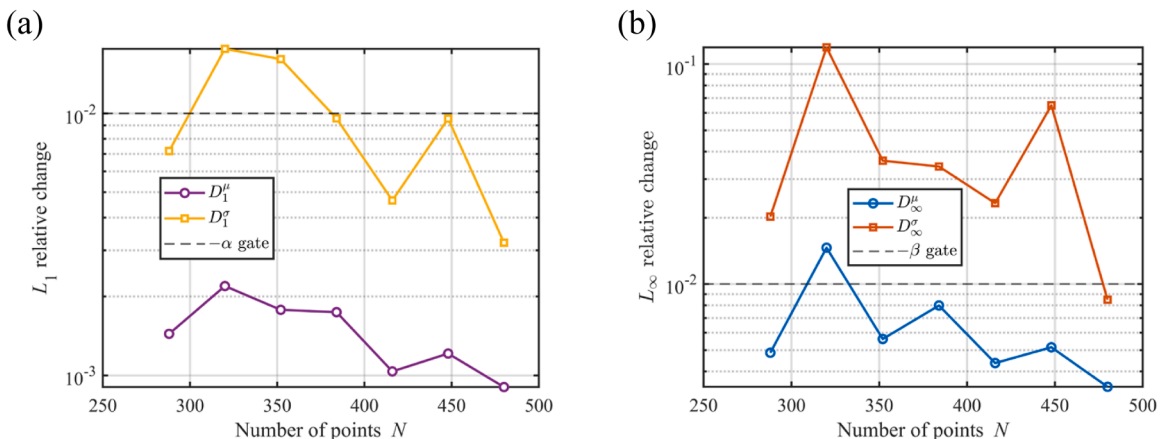


Fig. 2. Four different statistical magnitudes of moments at Sobol test set varying with simple size N .

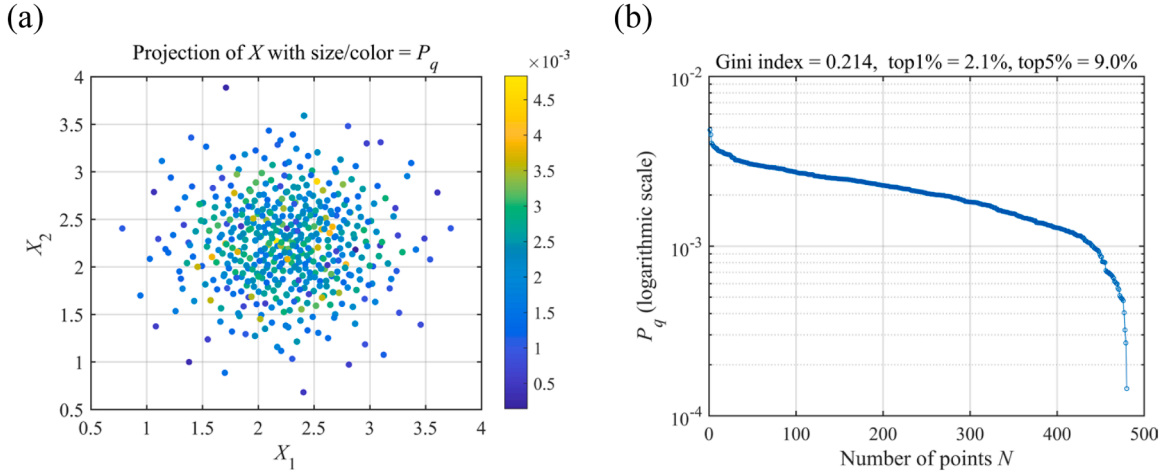


Fig. 3. (a) Spatial distribution of representative points and (b) assigned probabilities on a logarithmic scale.

$$\hat{\mu}(\theta) = \sum_{q=1}^N w_q(\theta) z_q, \hat{\sigma}(\theta) = \sqrt{\sum_{q=1}^N w_q(\theta) z_q^2 - \hat{\mu}^2(\theta)} \quad (26)$$

in which $w_q(\theta)$ denotes the reweighted assigned probabilities:

$$w_q(\theta) = \frac{P_q f(x_q | \theta)}{\phi(x_q)}, \quad \sum_{q=1}^N w_q(\theta) = 1, \quad (27)$$

where $f(x_q | \theta)$ and $\phi(x_q)$ denote the target joint PDF and the auxiliary probability density at x_q , respectively.

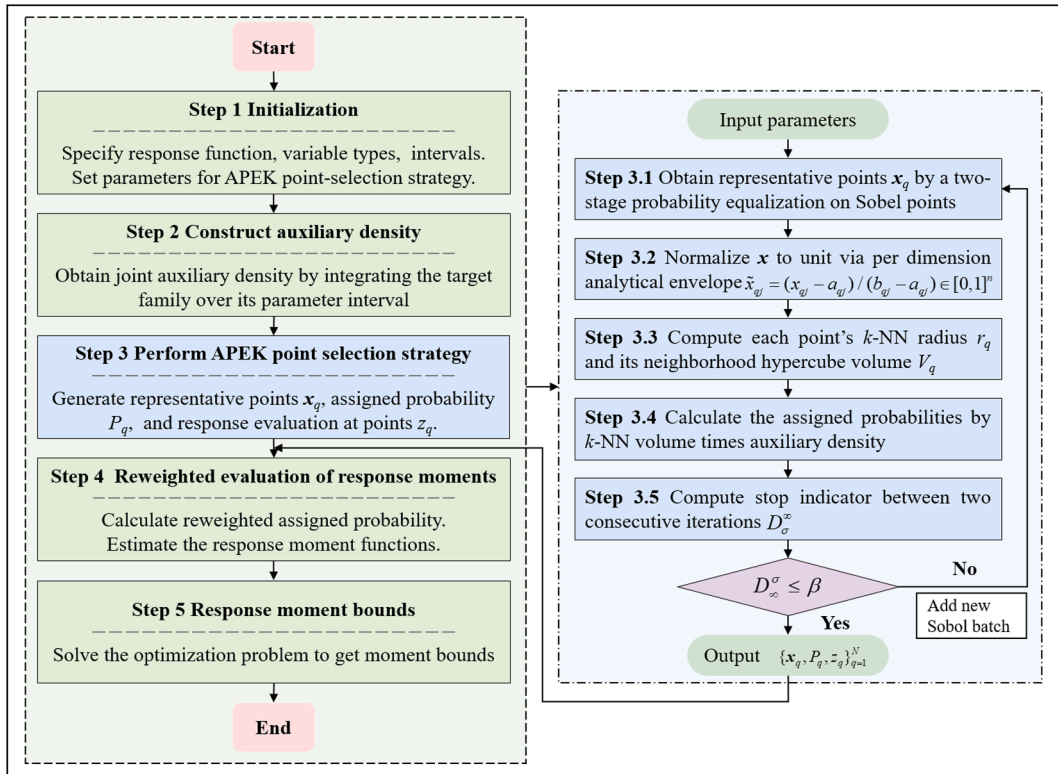


Fig. 4. Flowchart of the proposed adaptive SLRNI for estimating response moment functions and their bounds.

The extreme-value response moments for a dynamic structural system are also calculated by Eqs. (26) and (27), where z_q denotes the extreme-value response at points x_q .

(2) Response moment bounds

The mean and standard deviation bounds are obtained by solving the optimization problems in Eq. (14) and Eq. (15) over the domain of θ . Since the optimization objectives directly employ the reweighted formulas in Eq. (26), the computation of moment bounds requires no additional structural response evaluations. The starfish optimization algorithm [46] is employed for its strong global search ability and low sensitivity to design parameters.

Overall, the proposed framework transforms the estimation of response moments and their bounds under parametric p-boxes into a single-loop reweighted estimation. It is fully non-intrusive because it operates solely on probabilistic descriptions of uncertain inputs and treats the structural model as a black-box, without requiring explicit expressions or gradient information of the response function. With its non-intrusive nature and parallel capability, the proposed method exhibits strong competitiveness for complex engineering structures and is further validated in Section 4.

3.5. Implementation procedure

The procedure of the adaptive SLRNI method is summarized below and illustrated in Fig. 4.

Step 1: Initialization

Define the response function g and specify all uncertain inputs \mathbf{X} . For each imprecise random variable, define the distribution family and the bounds of the intervals θ . Set the algorithm parameters:

- the initial size $N_0 = 2^8 = 256$ provides a low-discrepancy starting set;
- the batch size $N_{\text{grow}} \in \{24, 32\}$ takes integer values; the maximum size $N_{\text{max}} = 4000$ provides a safe upper limit;
- the envelope multiplier $K \in \{6, 7, 8\}$ and the k -nearest-neighbor order $k \in \{6, 7, 8\}$ guarantee robust and well-conditioned neighborhood construction; the sensitivity of the hyperparameters K and k is examined in Appendix A, where the results confirm the robustness of the proposed method within the recommended parameter range;
- the number of Sobol test points M is selected in the integer interval $\{64, 96\}$.

Overall, these parameter choices offer a reliable balance between accuracy and computational efficiency.

Step 2: Construct the complete auxiliary density $\phi(\mathbf{x})$

For each input dimension, integrate the target family over its parameter interval to obtain the marginal PDF ϕ_j of the auxiliary density function. Multiply all marginals to form the joint density $\phi(\mathbf{x})$:

$$\phi(\mathbf{x}) = \phi_1 \phi_2 \cdots \phi_j, \phi_j = \frac{1}{\lambda_j} \int_{\mathcal{D}_{\theta_j}} f(x_j | \theta_j) d\theta_j, \text{ for } j = 1, 2, \dots, n.$$

Step 3: Perform APEK point-selection strategy

Step 3.1 Generate N_0 Sobol points in the unit cube. Perform a two-stage probability equalization process to obtain the representative points $x^{(0)}$, and compute the structural response at these points $z^{(0)}$. At iteration ℓ , the added Sobol batch performs the two-stage probability equalization transformation to obtain the new points x_{new}^ℓ . Evaluate the response at these new points: z_{new}^ℓ . The representative point set and response evaluations are updated as: $x^{(\ell)} = [x^{(\ell-1)}; x_{\text{new}}^\ell]$ and $z^{(\ell)} = [z^{(\ell-1)}; z_{\text{new}}^\ell]$.

Step 3.2 Compute per dimension analytical envelope $[a_j, b_j]$ based on the distribution family and parameter bounds. Normalize all coordinates to the unit interval: $\tilde{x}_{qj} = (x_{qj} - a_j) / (b_j - a_j) \in [0, 1]^n$.

Step 3.3 In the normalized space $\tilde{x}_q \in [0, 1]^n$, compute each point's k -nearest-neighbor radius r_q using Eq. (20). Then compute the local volume V_q of the neighborhood through Eq. (21).

Step 3.4 Evaluate the auxiliary density at \tilde{x}_q and calculate the assigned probabilities via Eq. (22).

Step 3.5 Compute the stopping indicator between two iterations using Eq. (24). If this indicator satisfies the target precision condition defined in Eq. (25), terminate the procedure and output the final data: $\{x_q, P_q, z_q\}_{q=1}^N$, where $N = N_0 + \ell N_{\text{grow}}$. Otherwise, the procedure returns to Steps 3.1–3.4.

Step 4: Response moment functions by reweighted evaluation

Calculate reweighted assigned probabilities $w_q(\theta)$ by Eq. (27) and estimate response mean and standard deviation functions via Eqs. (26).

Step 5: Response moment bounds via optimization

Compute the lower and upper bounds of response moments by solving the optimization problems defined in Eqs. (14) and (15). The starfish optimization algorithm [46] is employed in this study.

Remark 3. If all distribution parameters are crisp values, the hybrid uncertainty model reduces to a classic probability model. The proposed adaptive SLRNI framework is applicable to systems involving imprecise random variables, mixed imprecise-precise random uncertainties, and also to purely stochastic systems.

4. Examples

Four examples are presented to assess the accuracy, computational efficiency, and robustness of the proposed method. The first example is a mathematical benchmark problem, followed by a cantilever tube structure. The last two examples involve more complex structural systems: a 120-bar truss and a nonlinear offshore wind turbine tower.

4.1. Example 1: A test mathematical function

The response function of a mathematical problem is expressed as:

$$Y = g(X) = \sum_{i=1}^5 X_i^2$$

where $X_i \sim \mathcal{N}(\theta_1 \in [2, 2.5], \theta_2 \in [0.4, 0.45])$, θ_1 and θ_2 are the mean and standard deviation of input random variable X_i , respectively.

The mean and standard deviation of the output response Y , together with their relative errors with respect to the analytical solutions, are illustrated in Fig. 5 and Fig. 6. Note that the response moments with respect to interval parameters are calculated by fixing the other intervals at their midpoint values in all examples of this study. The relative errors between the proposed method and the exact solutions remain small (below 2%). Table 1 compares the bounds of response moments obtained using the proposed method, MCS-BGO (MCS combined with Bayesian global optimization), OSGNI [23] and OUDRM [22]. Although OSGNI and OUDRM improve computational efficiency compared with standard MCS, they only provide the bounds of response moments. In contrast, the proposed method accurately captures the full variation of the response moment functions over the interval parameter domain and provides more detailed statistical information than existing approaches.

Fig. 7 illustrates the evolution of the representative points during the point-selection iterations. The markers with different colors correspond to the initial Sobol batch of $N_0 = 256$ and the subsequent seven adaptive successive batches $x_{new}^{(\ell)}$ ($\ell = 1, \dots, 7$). As the iteration proceeds, the algorithm automatically inserts more points in the high-probability region around the mean of X_i , which explains the good accuracy obtained with a relatively small total number of model evaluations. The distribution of representative points gradually becomes more uniform as the representative set is enriched.

4.2. Example 2: A cantilever tube

To further verify the accuracy of the proposed method for structural application, a cantilever tube modified from Refs. [18,21] is analyzed, as illustrated in Fig. 8. The structure involves eight random variables, as listed in Table 2. The geometrical parameters are $L_1 = 115.75$ mm and $L_2 = 56.75$ mm.

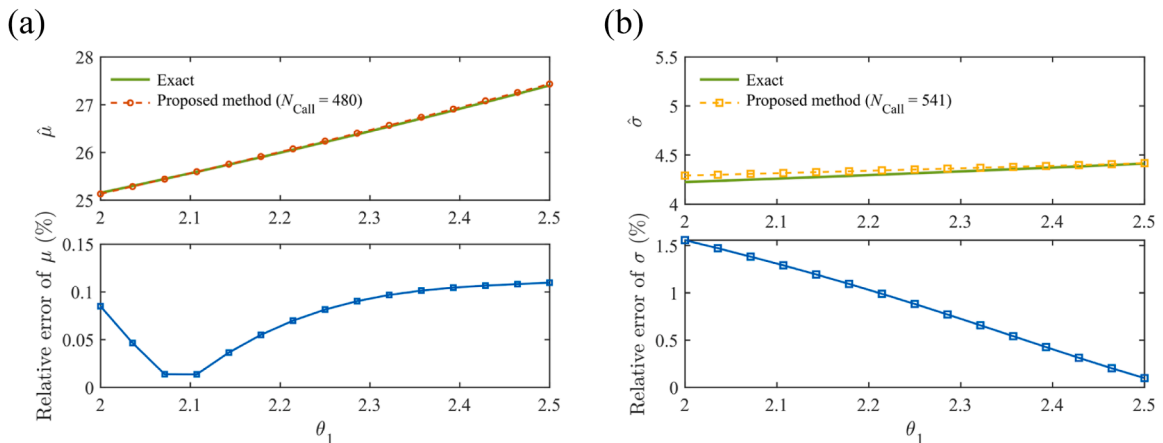


Fig. 5. (a) Mean $\hat{\mu}$ and (b) standard deviation $\hat{\sigma}$ of Y by adaptive SLRNI and their errors relative to exact results.

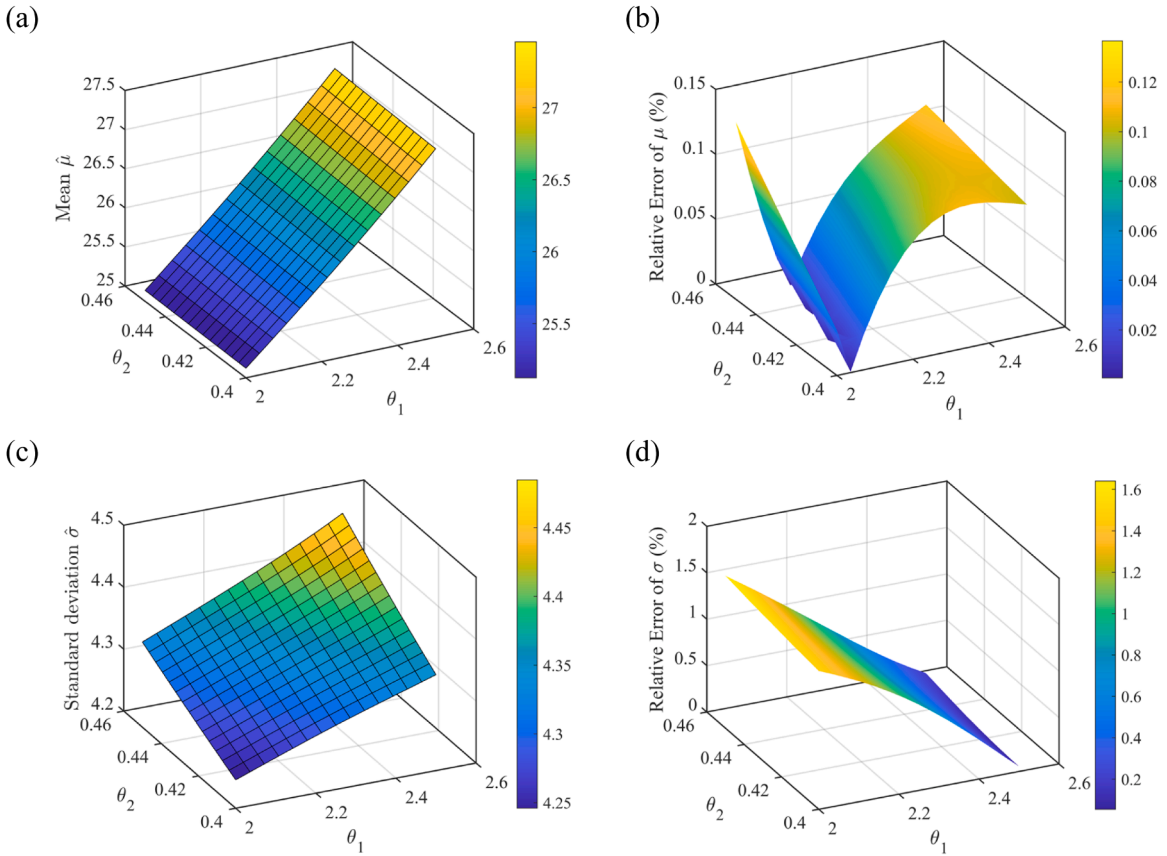


Fig. 6. Surfaces of response mean and standard deviation using the proposed method: (a) and (c), and their errors relative to exact results: (b) and (d).

Table 1
Mean and standard deviation bounds of output responses by several methods.

Methods	$\hat{\mu}^L$	$\hat{\mu}^U$	N_{Call}	$\hat{\sigma}^L$	$\hat{\sigma}^U$	N_{Call}
Exact result	20.80	32.26	—	3.61	5.07	—
MCS-BGO	20.80	32.03	20×10^6	3.62	5.04	23×10^6
OSGNI	20.80	32.26	3763	3.61	5.07	3763
OU DRM	20.80	32.26	1643	3.61	5.07	1643
Proposed method	20.79	32.14	480	3.66	5.08	480

Note: N_{call} refers to the number of response function evaluations required.

The response of interest is the maximum von Mises stress of the tube, defined as:

$$\sigma_{\max} = \sqrt{\sigma_x^2 + 3\tau_{zx}^2}, \tag{28}$$

in which σ_x and τ_{zx} denote the normal stress and shear stress, respectively, given by:

$$\sigma_x = \frac{P + F_1 \sin \varphi_1 + F_2 \sin \varphi_2}{A} + \frac{Md}{2I}, \tau_{zx} = \frac{Td}{4I} \tag{29}$$

where A , M and I are the cross-sectional area, bending moment, and moment of inertia, provided by:

$$A = \frac{\pi}{4} [d^2 - (d - 2t_c)^2], M = F_1 L_1 \cos \varphi_1 + F_2 L_2 \cos \varphi_2, I = \frac{\pi}{64} [d^4 - (d - 2t_c)^4] \tag{30}$$

The mean and standard deviation of the von Mises stress and their errors with respect to the MCS benchmark are presented in Fig. 9 and Fig. 10. The moment functions with respect to interval parameters are obtained by fixing the other intervals at their midpoint values. Table 3 summarizes the moment bounds estimated by MCS, Quasi-MCS-BGO (Quasi-MCS combined with Bayesian global

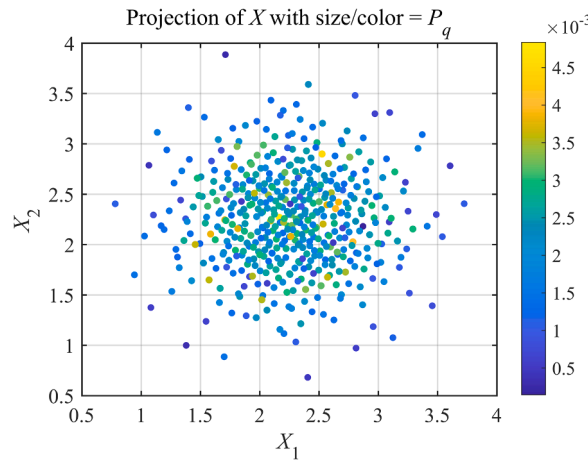


Fig. 7. Adaptive iterations of representative points in the input subspace (X_1, X_2) with $N_0 = 256$ and $N_{grow} = 32$.

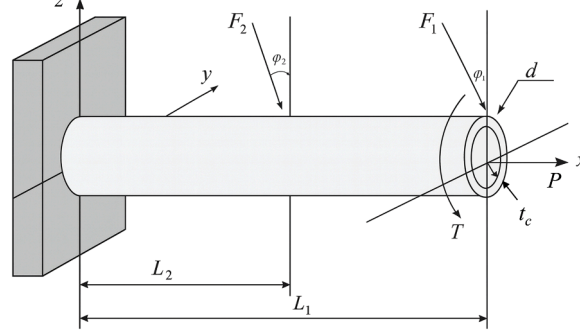


Fig. 8. A cantilever tube.

Table 2
Distribution types and parameters of input uncertain variables for cantilever tube.

Variables	Distribution types	Parameter γ^1	Parameter γ^2
P (N)	Uniform	10000	10100
T (N·m)	Uniform	80	85
$\phi 1(^{\circ})$	Normal	5	0.5
$\phi 2(^{\circ})$	Normal	10	1.0
F_1 (N)	Lognormal	$\theta_1 \in [2950, 3000]$	$\theta_2 \in [295, 300]$
F_2 (N)	Lognormal	$\theta_3 \in [2950, 3000]$	$\theta_4 \in [295, 300]$
t_c (mm)	Lognormal	$\theta_5 \in [5.0, 5.5]$	$\theta_6 \in [0.4, 0.6]$
d (mm)	Lognormal	$\theta_7 \in [40, 45]$	$\theta_8 \in [5.0, 6.0]$

Note: γ^1 and γ^2 represent the mean and standard deviation of random variables for Normal and Lognormal distribution types, while they correspond to the minimum and maximum values for Uniform distribution in this paper.

optimization), OSGNI, OUDRM and the proposed method. The proposed method achieves approximately one order-of-magnitude improvement in numerical efficiency compared with the benchmark methods. The proposed method possesses strong potential as a practical and powerful tool for engineering uncertainty quantification. Two additional engineering examples are presented next to further validate the effectiveness of the proposed method. Notably, Fig. 9 shows the Quasi-MCS results with $N_{Call} = 10^4$ yield satisfactory results. Considering the high computational cost of the following two complex examples, the Quasi-MCS results are adopted as the reference solutions for subsequent validation.

4.3. Example 3: Spatial truss FE structure

As shown in Fig. 11, a 120-bar spatial truss structure subjected to thirteen vertical concentrated loads is considered [47]. The truss structure is modeled as a three-dimensional FE model using the software framework OpenSees (<https://opensees.berkeley.edu>). The

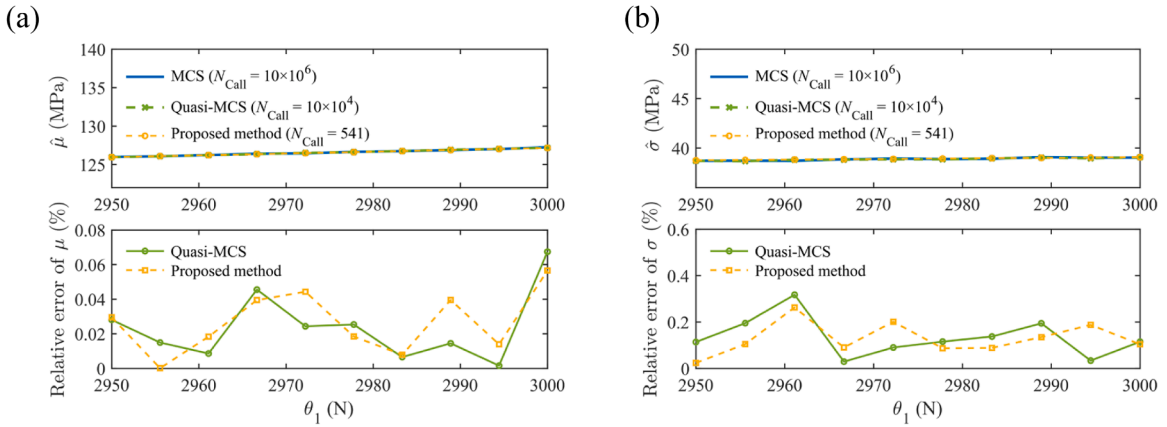


Fig. 9. (a) Mean and (b) standard deviation curves and their error curves relative to MCS reference.

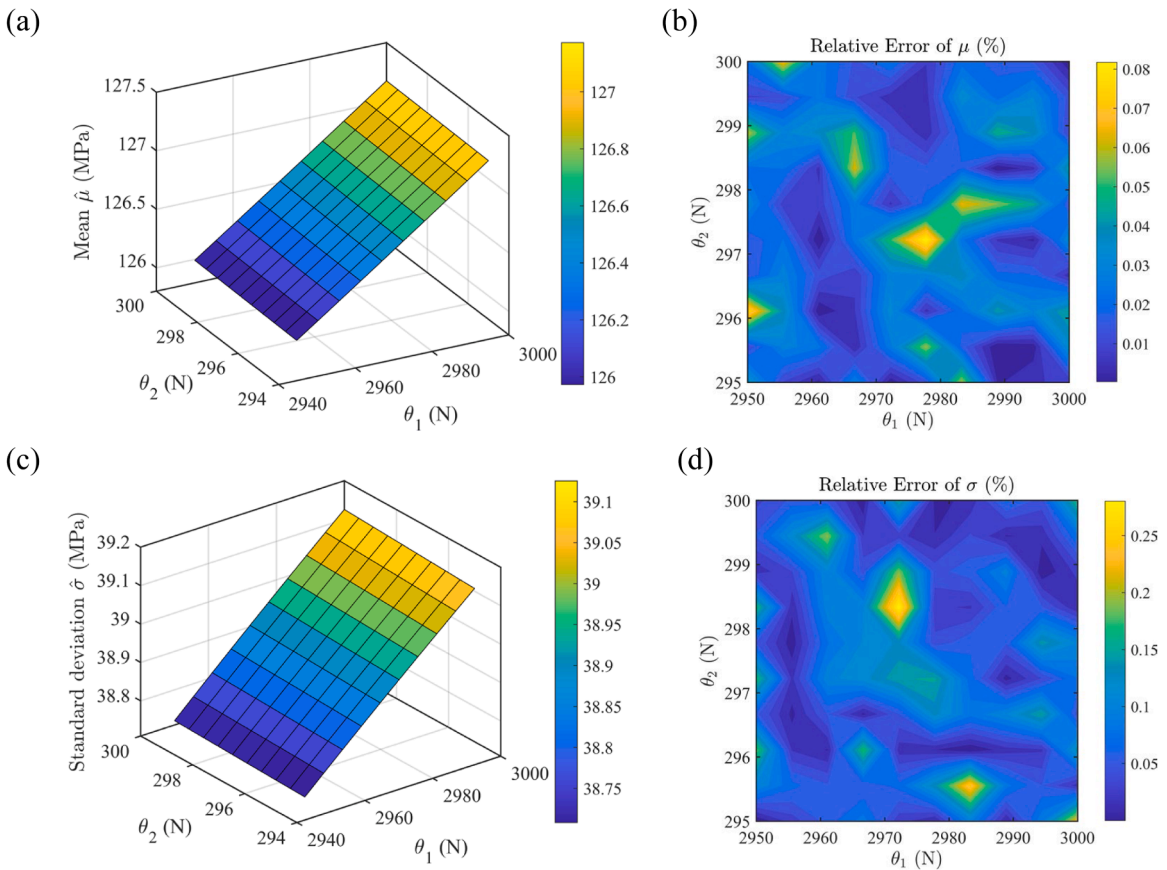


Fig. 10. Mean and standard deviation by proposed method ($N_{\text{Call}} = 572$): (a) and (c), and their errors relative to MCS reference with $N_{\text{Call}} = 100 \times 10^6$: (b) and (d).

FE model consists of 49 nodes and 120 elements. All elements are assumed to have the same cross-sectional area A and Young's modulus E . Thirteen static vertical concentrated loads P_0, P_1, \dots, P_{12} (kN) are applied to nodes 0–12 (integer values). The distribution types and parameters of input uncertain variables are displayed in Table 4.

The response of interest is the vertical displacement of node. The corresponding response function is:

$$g = V_1(E, A, P_0, P_1, \dots, P_{12}). \tag{31}$$

As shown in Fig. 12, Fig. 13 and Table 5, the estimated moments of the vertical displacement at node 0, as well as their bounds, are

Table 3
Mean and standard deviation bounds of von Mises stress obtained by several methods.

Methods	$\hat{\mu}^l$ (MPa)	$\hat{\mu}^U$ (MPa)	N_{Call}	$\hat{\sigma}^l$ (MPa)	$\hat{\sigma}^U$ (MPa)	N_{Call}
MCS-BGO	105.37	154.60	14×10^6	27.77	55.63	16×10^6
Quasi-MCS-BGO	105.48	154.26	18×10^4	27.66	55.63	27×10^4
OSGNI	105.44	154.41	11592	27.52	55.83	10304
OU DRM	105.42	154.32	3528	27.27	54.96	3136
Proposed method	105.32	154.38	572	27.68	56.53	572

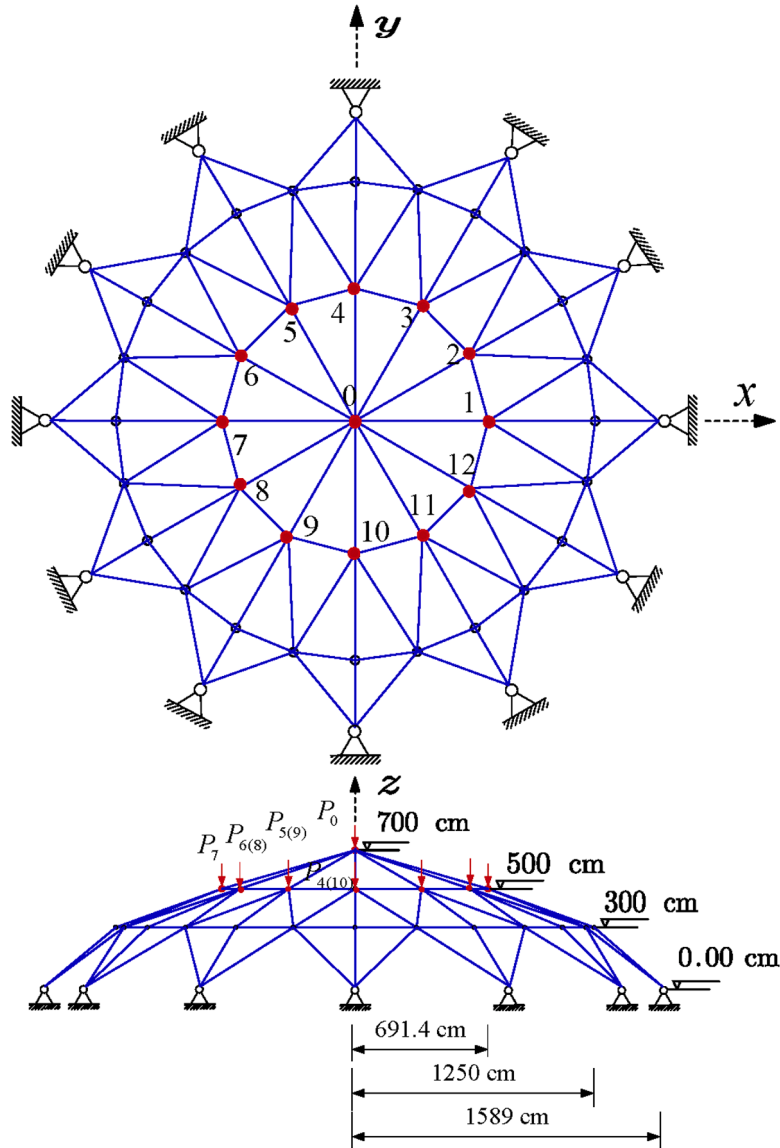


Fig. 11. Top and side views for a 120-bar space truss structure.

in close agreement with the Quasi-MCS benchmark. This case study verifies the accuracy and efficiency of the proposed method for complex FE structures through comparison with several existing approaches. From Table 5, the number of representative points required by the proposed approach increases as the stopping indicator β decreases from 0.01 to 0.008 in the iterative criterion, resulting in improved accuracy.

In terms of model evaluations, Quasi-MCS requires 1.8×10^5 and 1.9×10^5 FE model calls for estimating the mean and standard deviation, respectively, whereas the proposed approach requires only 1.24×10^3 evaluations for both quantities. This corresponds to

Table 4
Distribution information of input uncertainty variables for truss structure.

Random variable	Distribution	Parameter γ^1	Parameter γ^2
E (GPa)	Gamma	180	200
A (mm ²)	Uniform	1600	1800
$P_{1(2,4,5,7,8,10,11)}$ (kN)	Lognormal	250	25
P_0 (kN)	Lognormal	$\theta_1 \in [240, 280]$	$\theta_2 \in [24, 28]$
P_3 (kN)	Lognormal	$\theta_3 \in [240, 280]$	$\theta_4 \in [24, 28]$
P_6 (kN)	Lognormal	$\theta_5 \in [240, 280]$	$\theta_6 \in [24, 28]$
P_9 (kN)	Lognormal	$\theta_7 \in [240, 280]$	$\theta_8 \in [24, 28]$
P_{12} (kN)	Lognormal	$\theta_9 \in [240, 280]$	$\theta_{10} \in [24, 28]$

Note: γ^1 and γ^2 represent the mean and standard deviation of random variables for Gamma distribution type.

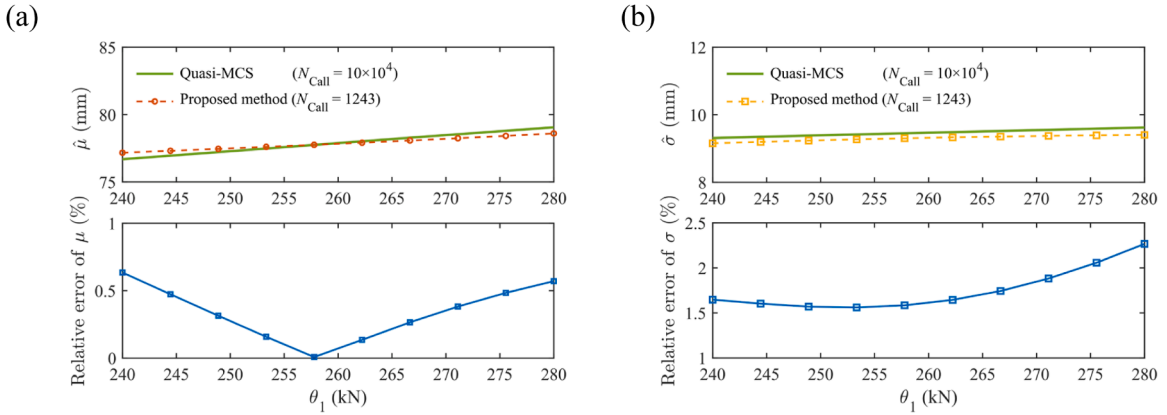


Fig. 12. (a) Means and (b) standard deviations of vertical displacements using the proposed method and errors relative to Quasi-MCS reference.

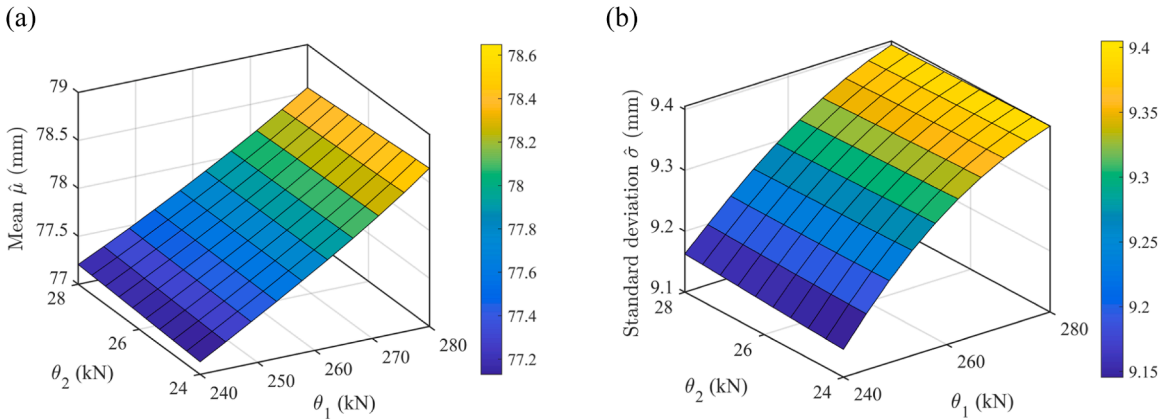


Fig. 13. 3D surfaces of displacement (a) mean and (b) standard deviation by the proposed method with $N_{Call} = 1243$.

nearly two orders of magnitude reduction ($\approx 99.3\%$ fewer model calls). Different Quasi-MCS sample sizes are used for the mean and standard deviation because their optimization objectives correspond to different functions over the interval parameter domain, which exhibit different convergence behaviors. The OSGNI and OUDRM do not provide complete moment functions and require 20244 and 7644 model evaluations, while the proposed method reduces the computational cost by approximately 94% and 84% relative to these two methods. These results demonstrate the efficiency and robustness of the proposed approach for hybrid-uncertainty analysis of complex structural systems.

4.4. Example 4: Offshore wind turbine tower

As shown in Fig. 14, the monopile offshore wind turbine tower is idealized as a three degree-of-freedom (DOF) lateral shear-type nonlinear system supported by an elastic soil spring at the mudline [48]. The turbine is subjected to wind and wave loads at the top and

Table 5
Mean and standard deviation bounds of vertical displacements obtained by several methods.

Methods	$\bar{\mu}^L$ (mm)	$\bar{\mu}^U$ (mm)	N_{Call}	$\bar{\sigma}^L$ (mm)	$\bar{\sigma}^U$ (mm)	N_{Call}
Quasi-MCS-BGO	75.14	80.88	18×10^4	9.02	9.85	19×10^4
OSGNI	75.19	80.80	20244	8.61	9.24	20244
OUDRM	75.21	80.81	7644	8.85	9.52	7644
Proposed method ($\beta = 0.01$)	76.43	79.58	1243	8.80	9.98	1243
Proposed method ($\beta = 0.008$)	76.40	79.71	1744	8.80	9.84	1744

lowest DOFs, respectively. The tower height is $H = 90$ m with equal story height $h = H/3 = 30$ m; rotor radius is $R = 63$ m; elastic modulus is $E = 210$ GPa; baseline bending rigidity is $EI_0 = 3.0 \times 10^{10} \text{N} \cdot \text{m}^2$. Six imprecise random variables and six precise random inputs are considered for the tower, as listed in Table 6.

The generalized displacements $u(t) = [u_1(t), u_2(t), u_3(t)]^T$ correspond to heights $z = \{h, 2h, 3h\}$ along the tower. The response of interest is the peak displacement at the top, which is calculated by using the implicit Newmark integration scheme combined with Newton-Raphson iterations. The time domain is $t \in [0, 180]$ with a constant time step of $\Delta t = 0.01$ s.

The nonlinear equation of motion governing the structural response is given by:

$$M\ddot{u}(t) + C\dot{u}(t) + Ku(t) + f_{nl}(u(t)) = F(t), \tag{32}$$

where M , C and K are mass, stiffness, and damping matrices; $f_{nl}(u(t))$ represents the nonlinear restoring force; $F(t)$ denotes the environmental excitation. The detailed descriptions of these components are provided in the Appendix B.

To verify the accuracy of the proposed method for nonlinear dynamic problems, its results are compared with the benchmark solutions obtained using Quasi-MCS, as shown in Fig. 15, Fig. 16 and Table 7. The proposed adaptive SLRNI method provides accurate and efficient evaluation of the response statistics for the nonlinear dynamic system. In contrast, OSGNI and OUDRM exhibit noticeable deviations, partly due to their reliance on gradient-based optimization and linearized integration schemes, as listed in Table 7. For nonlinear and time-dependent responses, these approaches are susceptible to local convergence and numerical errors associated with low-order polynomial approximations, which may lead to biased statistical estimates.

The adaptive SLRNI performs single-loop reweighted integration and eliminates the need for nested optimization or sparse-grid discretization. This improves numerical stability, convergence behavior, and computational efficiency, making the approach suitable for nonlinear and dynamic systems with strong coupling effects.

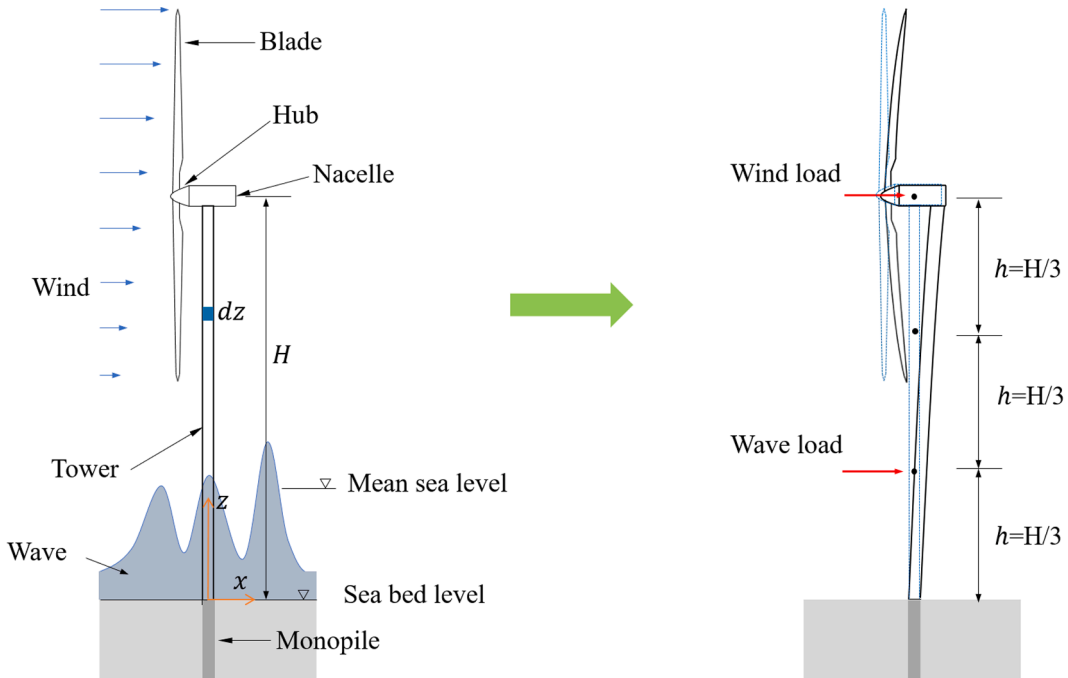


Fig. 14. Configuration of the monopile offshore wind turbine tower and its equivalent simplified structural mode.

Table 6
Distribution information of input uncertainty variables.

Uncertain variables	Distribution types	Parameter γ^1	Parameter γ^2
k_v	Normal (truncated to $[0, +\infty)$)	1.0	0.1
H_s (m)	Lognormal	3.0	0.6
f_p	Uniform	0.08	0.14
Ψ_w	Uniform	0.90	1.10
I_u	Normal (truncated to $[0, +\infty)$)	0.15	0.03
ρ_{air} (kg/m ³)	Normal (truncated to $[0, +\infty)$)	1.225	0.05
k_{soil} ($\times 10^8$ N/m)	Gamma	$\theta_1 \in [1.2, 2.2]$	$\theta_2 \in [0.2, 0.6]$
ζ	Gamma	$\theta_3 \in [0.015, 0.030]$	$\theta_4 \in [0.005, 0.010]$
C_T	Lognormal	$\theta_5 \in [0.80, 0.92]$	$\theta_6 \in [0.06, 0.10]$
m_{nac} ($\times 10^5$ kg)	Gamma	$\theta_7 \in [3.2, 3.8]$	$\theta_8 \in [0.3, 0.5]$
m_{tow} ($\times 10^5$ kg)	Gamma	$\theta_9 \in [1.9, 2.5]$	$\theta_{10} \in [0.2, 0.4]$
ρ_s (kg/m ³)	Gamma	$\theta_{11} \in [7800, 8050]$	$\theta_{12} \in [100, 200]$

Note: the definitions of all symbols are provided in the Appendix.

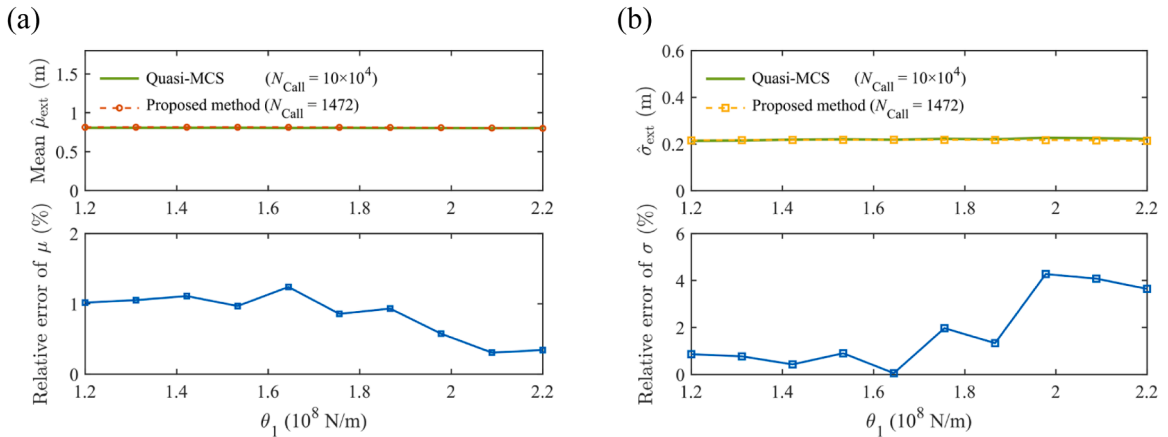


Fig. 15. Mean and standard deviation curves of peak displacement at top and errors relative to Quasi-MCS reference.

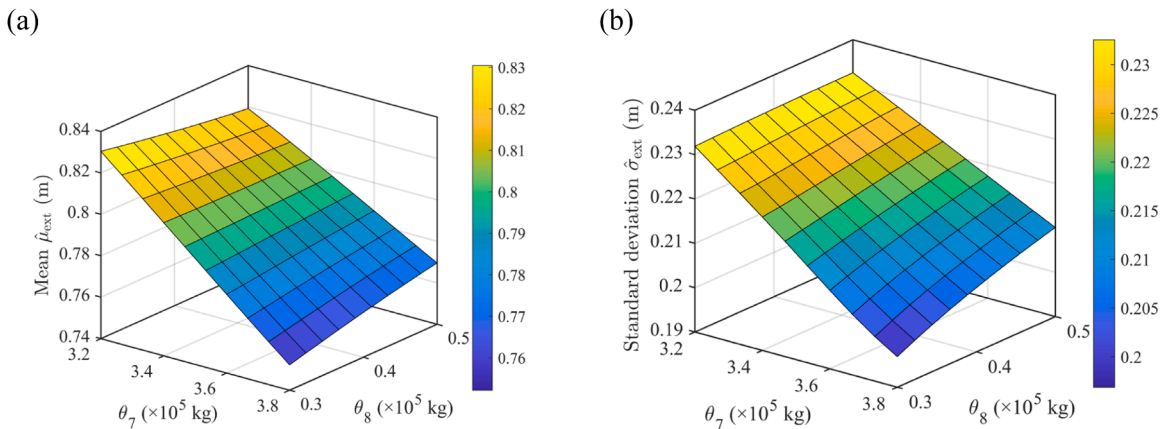


Fig. 16. Moment surfaces of peak displacements by proposed approach ($N_{\text{Call}} = 1472$): (a) mean; (b) standard deviation.

5. Conclusions

To estimate response moment functions and their bounds for structures under parametric p-boxes, this study proposes an adaptive single-loop reweighted numerical integration (adaptive SLRNI) approach. Expressions for the response moments are derived from the generalized probability density integral equations (PDIEs) and reformulated through a reweighting strategy based on a complete auxiliary density. The resulting reweighted formulation is combined with an adaptive probability-equalized k -nearest-neighbor

Table 7
Mean and standard deviation bounds of peak displacements by several methods.

Method	$\hat{\mu}_{\text{res}}^L$ (m)	$\hat{\mu}_{\text{res}}^U$ (m)	N_{Call}	$\hat{\sigma}_{\text{res}}^L$ (m)	$\hat{\sigma}_{\text{res}}^U$ (m)	N_{Call}
Quasi-MCS-BGO	0.664	1.018	31×10^4	0.157	0.332	27×10^4
OSGNI	0.537	0.965	39964	0.000	0.287	48500
OU DRM	0.683	1.384	18463	0.201	0.270	5994
Proposed method	0.666	0.980	1472	0.155	0.324	1472

(APEK) point-selection technique to evaluate response moment functions and their bounds in a single-loop computational framework. The proposed framework is non-intrusive and applicable to black-box models and complex engineering systems. Four representative examples, including a mathematical problem, a cantilever tube, a 120-bar truss, and a nonlinear offshore wind turbine tower, are investigated to assess the performance of the proposed approach. The primary findings are summarized as follows.

- (1) The proposed method provides accurate estimates of response moment functions and their bounds under hybrid uncertainties. For general structural systems, the errors in the estimated moments remain within approximately 2%, whereas those for finite element and nonlinear dynamic systems remain within about 6%. By contrast, some gradient-based approaches may converge to local optima for nonlinear structures, thereby leading to noticeable estimation errors.
- (2) The proposed approach substantially reduces the number of structural model evaluations compared with existing methods. The adaptive SLRNI reduces model evaluations by approximately 99% compared with Quasi-MCS, and by roughly 80% and 90% relative to OSGNI and OU DRM, respectively. This improvement in efficiency, while maintaining comparable accuracy, demonstrates the computational advantage of the proposed approach.
- (3) The adaptive SLRNI incorporates an adaptive enrichment strategy and supports parallel computation. The APEK point-selection strategy generates uniformly distributed representative points with balanced probability weights. It enables accurate reweighted integration and allows incremental enrichment based on a prescribed convergence criterion.

Overall, the adaptive SLRNI is developed within the basis of the direct probability integral method, which provides a flexible and effective framework for hybrid aleatory-epistemic uncertainty quantification in advanced computational mechanics. The proposed approach is primarily intended for problems involving a moderate number of random and interval variables, since the performance of both the auxiliary density function and the APEK strategy may deteriorate in very high-dimensional settings. Future work will focus on developing more efficient adaptive point-selection strategies and incorporating surrogate modeling or active learning techniques to improve scalability. Additional research directions include extensions to reliability analysis, sensitivity analysis, reliability-based design optimization, and the quantification of instantaneous response probability density functions for dynamic systems under hybrid uncertainties. Extensions to dependent epistemic variables described by general convex constraint sets also constitute a promising direction for future research.

CRedit authorship contribution statement

Jiaran Liu: Writing – original draft, Visualization, Software, Methodology, Formal analysis, Conceptualization. **Marcos A. Valdebenito:** Writing – review & editing, Supervision, Methodology, Formal analysis, Conceptualization. **Dixiong Yang:** Writing – review & editing, Supervision, Methodology, Funding acquisition, Conceptualization. **Matthias G.R. Faes:** Writing – review & editing, Supervision, Methodology, Funding acquisition, Conceptualization.

Declaration of competing interest

The authors declare that they have no known competing financial interests or personal relationships that could have appeared to influence the work reported in this paper.

Acknowledgments

Jiaran Liu acknowledges the financial support of the China Scholarship Council (Project No: 202406060246). Dixiong Yang would like to acknowledge the financial support of the National Natural Science Foundation of China (Grant Nos. 12032008 and 52378484). Matthias G.R. gratefully acknowledges the financial support of the German Research Foundation (DFG) (Grant No. 530326817).

Appendix A. Sensitivity of hyperparameters K and k

To examine the robustness of the proposed method with respect to the envelope multiplier K and number of nearest neighbors k , a sensitivity study is conducted for Example 1. The parameters are varied within the recommended integer range $K, k \in \{6, 7, 8\}$, and the resulting moment bounds and model evaluations are reported in [Table A1](#).

Table A1

Sensitivity analysis of hyperparameters K and k for the proposed method (Example 1).

K	k	$\hat{\mu}^L$	$\hat{\mu}^U$	$\hat{\sigma}^L$	$\hat{\sigma}^U$	N_{Call}
6	8	20.79	32.14	3.66	5.08	480
6	7	20.84	32.15	3.62	5.13	542
6	6	20.84	32.17	3.64	5.09	542
7	6	20.84	32.17	3.64	5.09	542
8	6	20.84	32.17	3.64	5.09	542
8	7	20.84	32.15	3.62	5.13	542
8	8	20.80	32.14	3.66	5.08	480

The results indicate negligible variations in the estimated mean and standard deviation bounds across the tested parameter combinations. The differences are mainly reflected in the number of model evaluations, confirming that the recommended range provides stable and reliable performance.

Appendix B. Mass, stiffness, damping and loads for wind turbine tower

(1) Mass

The total tower steel mass m_{tower} is evenly lumped to the three stories and nacelle mass m_{nac} is added at the top DOF. The mass matrix is given by:

$$M = \text{diag}(m_1, m_2, m_3), m_1 = m_2 = \frac{m_{\text{tower}}}{3}, m_3 = \frac{m_{\text{tower}}}{3} + m_{\text{nac}}.$$

(2) Stiffness

The linear stiffness is scaled to match the target fundamental frequency $f_1^{\text{tgt}} = 0.3 \text{ Hz}$: $K = \gamma_K K_p, \gamma_K = (2\pi f_1^{\text{tgt}})^2 / \omega_{1,p}^2$, where K_p starts from a tri-diagonal prototype with story stiffness k_{story} and the soil spring k_{soil} at the base:

$$K_p = \begin{bmatrix} k_{\text{soil}} + k_{\text{story}} & -k_{\text{story}} & 0 \\ -k_{\text{story}} & 2k_{\text{story}} & -k_{\text{story}} \\ 0 & -k_{\text{story}} & k_{\text{story}} \end{bmatrix}.$$

(3) Damping

The damping uses Rayleigh form $C = \alpha_M M + \beta_K K$. The coefficients $\{\alpha_M, \beta_K\}$ are determined by matching the epistemically uncertain modal damping ratio ζ at the 1st and 3rd modes with natural frequencies $\{\omega_A, \omega_B\}$:

$$\begin{bmatrix} \frac{1}{2\omega_A} & \frac{\omega_A}{2} \\ \frac{1}{2\omega_B} & \frac{\omega_B}{2} \end{bmatrix} \begin{bmatrix} \alpha_M \\ \beta_K \end{bmatrix} = \begin{bmatrix} \zeta \\ \zeta \end{bmatrix}.$$

(4) Nonlinear duffing restoring at the top DOF is adopted:

$$f_{\text{nl}}(\mathbf{u}) = [0, 0, \alpha_3 u_3^3]^T, \alpha_3 \geq 0 (\text{N} / \text{m}^3),$$

where $\alpha_3 = rK_{33} / u_{\text{ref}}^2$ and set $r = 0.2, u_{\text{ref}} = 0.30 \text{ m}$.

(5) Environmental loads

· Wind load at hub (DOF 3): $F_3(t)$.

The instantaneous aerodynamic thrust is modeled as mean plus turbulent fluctuation:

$$F_3(t) = T_{\text{mean}} [1 + I_u u_r(t)], \quad T_{\text{mean}} = \frac{1}{2} C_T \rho_{\text{air}} A_{\text{rot}} V_{\text{mean}}^2,$$

where T_{mean} is mean thrust; I_t is turbulence intensity; $u_t(t)$ is zero-mean, unit-standard-deviation stochastic fluctuation obtained by low-pass filtering white noise; C_T is thrust coefficient; ρ_{air} is air density; $A_{\text{rot}} = \pi R^2$ is rotor swept area; $V_{\text{mean}} = 10$ m/s is reference mean wind speed.

·Wave load at the lowest DOF (DOF 1): $F_1(t)$

Wave load is represented by a lateral Morison-type force by a narrowband random process synthesized as a sum of random-phase sinusoids:

$$F_1(t) = \frac{A(H_s, \Psi_w)}{N_h} \sum_{k=1}^{N_h} \sin(2\pi f_k t + \Phi_k), \quad f_k \sim N\left(f_p, \left(\gamma f_p\right)^2\right), \quad \Phi_k \sim U[0, 2\pi],$$

where H_s is the significant wave height and Ψ_w is an amplitude factor; $N_h = 20$ is the number of synthesized harmonics; f_k and Φ_k are frequency and phase, which are normally and uniformly distributed, respectively; f_p is wave frequency for narrowband synthesis. $\gamma = 0.2$ is the spectral bandwidth parameter.

Data availability

Data will be made available on request.

References

- [1] A. Der Kiureghian, O. Ditlevsen, Aleatory or epistemic? Does it matter? *Struct Saf* 31 (2009) 105–112, <https://doi.org/10.1016/j.strusafe.2008.06.020>.
- [2] M. Beer, S. Ferson, V. Kreinovich, Imprecise probabilities in engineering analyses, *Mech Syst Signal Process* 37 (2013) 4–29, <https://doi.org/10.1016/j.ymssp.2013.01.024>.
- [3] P.P. Li, M.A. Valdebenito, C. Dang, M. Beer, MGR. Faes, Aleatory and epistemic uncertainty in reliability analysis: an engineering perspective, *Struct Saf* 119 (2026) 102666, <https://doi.org/10.1016/j.strusafe.2025.102666>.
- [4] W.L. Oberkampf, J.C. Helton, C.A. Joslyn, S.F. Wojtkiewicz, S. Ferson, Challenge problems: uncertainty in system response given uncertain parameters, *Reliab Eng Syst Saf* 85 (2004) 11–19, <https://doi.org/10.1016/j.res.2004.03.002>.
- [5] AP. Dempster, Upper and lower probabilities induced by a multivalued mapping, *Ann Math Stat* 38 (1967) 325–339, <https://doi.org/10.1214/aoms/1177698950>.
- [6] G. Shafer, *A Mathematical Theory of Evidence*, Princeton University Press, 1976, <https://doi.org/10.2307/j.ctv10vm1qb>.
- [7] P. Soundappan, E. Nikolaidis, R.T. Haftka, R. Grandhi, R. Canfield, Comparison of evidence theory and Bayesian theory for uncertainty modeling, *Reliab Eng Syst Saf* 85 (2004) 295–311, <https://doi.org/10.1016/j.res.2004.03.018>.
- [8] J.C. Helton, J.D. Johnson, W.L. Oberkampf, CB. Storlie, A sampling-based computational strategy for the representation of epistemic uncertainty in model predictions with evidence theory, *Comput Methods Appl Mech Eng* 196 (2007) 3980–3998, <https://doi.org/10.1016/j.cma.2006.10.049>.
- [9] LA. Zadeh, Fuzzy sets as a basis for a theory of possibility, *Fuzzy Sets Syst* 1 (1978) 3–28, [https://doi.org/10.1016/0165-0114\(78\)90029-5](https://doi.org/10.1016/0165-0114(78)90029-5).
- [10] D. Dubois, H. Prade, *Possibility Theory*, Plenum Press, New York, 1988.
- [11] S. Gudder, Fuzzy Probability Theory, *Demonstr Math* 31 (1998) 235–254, <https://doi.org/10.1515/dema-1998-0128>.
- [12] P. Agarwal, DHS. Nayal, Possibility theory versus probability theory in fuzzy measure theory, *Int J Eng Res Appl* 5 (2015) 37–43.
- [13] S. Ferson, V. Kreinovich, L. Ginzburg, F. Sentz, *Constructing Probability Boxes and Dempster-Shafer Structures*, Sandia National Laboratories, Morgantown, CA, USA, 2003, <https://doi.org/10.2172/809606>.
- [14] S. Destercke, D. Dubois, E. Chojnacki, Unifying practical uncertainty representations: I. generalized p-boxes, *Int J Approx Reason* 49 (2008) 649–663, <https://doi.org/10.1016/j.ijar.2008.07.003>.
- [15] M.C.M. Troffaes, S. Destercke, Probability boxes on totally preordered spaces for multivariate modelling, *Int J Approx Reason* 52 (2011) 767–791, <https://doi.org/10.1016/j.ijar.2011.02.001>.
- [16] V. Hoang, B. Rosic, H. Matthies, Characterization and propagation of uncertainties associated with limited data using a hierarchical parametric probability box, *Proc Appl Math Mech* 18 (2018) e201800475, <https://doi.org/10.1002/pamm.201800475>.
- [17] R. Schöbi, B. Sudret, Structural reliability analysis for p-boxes using multi-level meta-models, *Probabilistic Eng Mech* 48 (2017) 27–38, <https://doi.org/10.1016/j.probengmech.2017.04.001>.
- [18] MC. Bruns, *Propagation of imprecise probabilities through black box models*, Georgia Institute of Technology, 2006. M.S. thesis.
- [19] H. Zhang, R.L. Mullen, RL. Muhanna, Structural analysis with probability-boxes, *Int J Reliab Saf* 6 (2012) 110–129, <https://doi.org/10.1504/IJRS.2012.044292>.
- [20] M. Bruns, C.J.J. Paredis, Numerical Methods for Propagating Imprecise Uncertainty, *American Society of Mechanical Engineers Digital Collection* (2008) 1077–1091, <https://doi.org/10.1115/DETC2006-99237>.
- [21] Z. Xiao, X. Han, C. Jiang, G. Yang, An efficient uncertainty propagation method for parameterized probability boxes, *Acta Mech* 227 (2016) 633–649, <https://doi.org/10.1007/s00707-015-1492-2>.
- [22] H.B. Liu, C. Jiang, X.Y. Jia, X.Y. Long, Z. Zhang, F.J. Guan, A new uncertainty propagation method for problems with parameterized probability-boxes, *Reliab Eng Syst Saf* 172 (2018) 64–73, <https://doi.org/10.1016/j.res.2017.12.004>.
- [23] H.B. Liu, C. Jiang, J. Liu, J.Z. Mao, Uncertainty propagation analysis using sparse grid technique and saddlepoint approximation based on parameterized p-box representation, *Struct Multidiscip Optim* 59 (2019) 61–74, <https://doi.org/10.1007/s00158-018-2049-5>.
- [24] H.B. Liu, M. Chen, C. Du, J.C. Tang, C.M. Fu, GL. She, A copula-based uncertainty propagation method for structures with correlated parametric p-boxes, *Int J Approx Reason* 138 (2021) 89–104, <https://doi.org/10.1016/j.ijar.2021.08.002>.
- [25] N. Pedroni, E. Zio, Hybrid uncertainty and sensitivity analysis of the model of a twin-jet aircraft, *J Aerosp Inf Syst* 12 (2015) 73–96, <https://doi.org/10.2514/1.1010265>.
- [26] C. Ding, C. Dang, M. Broggi, M. Beer, Estimation of response expectation bounds under parametric p-boxes by combining Bayesian global optimization with unscented transform, *ASCE-ASME J Risk Uncertain Eng Syst Part Civ Eng* 10 (2024), <https://doi.org/10.1061/AJRUA6/RUENG-1169>.
- [27] P.F. Wei, Z.Z. Lu, J.W. Song, Extended Monte Carlo simulation for parametric global sensitivity analysis and optimization, *AIAA J* 52 (2014), <https://doi.org/10.2514/1.J052726>.

- [28] P.F. Wei, J.W. Song, S.F. Bi, M. Broggi, M. Beer, Z.Z. Lu, et al., Non-intrusive stochastic analysis with parameterized imprecise probability models: I. Performance estimation, *Mech Syst Signal Process* 124 (2019) 349–368, <https://doi.org/10.1016/j.ymssp.2019.01.058>.
- [29] R. Schöbi, B. Sudret, Global sensitivity analysis in the context of imprecise probabilities (p-boxes) using sparse polynomial chaos expansions, *Reliab Eng Syst Saf* 187 (2019) 129–141, <https://doi.org/10.1016/j.res.2018.11.021>.
- [30] H.B. Liu, C. Jiang, Z. Xiao, Efficient uncertainty propagation for parameterized p-box using sparse-decomposition-based polynomial chaos expansion, *Mech Syst Signal Process* 138 (2020) 106589, <https://doi.org/10.1016/j.ymssp.2019.106589>.
- [31] P.F. Wei, F.C. Liu, M. Valdebenito, M. Beer, Bayesian probabilistic propagation of imprecise probabilities with large epistemic uncertainty, *Mech Syst Signal Process* 149 (2021) 107219, <https://doi.org/10.1016/j.ymssp.2020.107219>.
- [32] P.F. Wei, F.Q. Hong, K.K. Phoon, M. Beer, Bounds optimization of model response moments: a twin-engine Bayesian active learning method, *Comput Mech* 67 (2021) 1273–1292, <https://doi.org/10.1007/s00466-021-01977-8>.
- [33] C. Dang, P.F. Wei, M.G.R. Faes, M. Beer, Bayesian probabilistic propagation of hybrid uncertainties: estimation of response expectation function, its variable importance and bounds, *Comput Struct* 270 (2022) 106860, <https://doi.org/10.1016/j.compstruc.2022.106860>.
- [34] G.H. Chen, D.X. Yang, Direct probability integral method for stochastic response analysis of static and dynamic structural systems, *Comput Methods Appl Mech Eng* 357 (2019) 112612, <https://doi.org/10.1016/j.cma.2019.112612>.
- [35] G.H. Chen, D.X. Yang, A unified analysis framework of static and dynamic structural reliabilities based on direct probability integral method, *Mech Syst Signal Process* 158 (2021) 107783, <https://doi.org/10.1016/j.ymssp.2021.107783>.
- [36] R. Pang, D. Zai, B. Xu, J. Liu, C. Zhao, Q. Fan, et al., Stochastic dynamic and reliability analysis of AP1000 nuclear power plants via DPIM subjected to mainshock-aftershock sequences, *Reliab Eng Syst Saf* 235 (2023) 109217, <https://doi.org/10.1016/j.res.2023.109217>.
- [37] H.S. Chen, Y.X. Gao, D.X. Yang, Z. Meng, Z.J. Fu, A novel weight index-based uniform partition technique of multi-dimensional probability space for structural uncertainty quantification, *Comput Methods Appl Mech Eng* 431 (2024) 117297, <https://doi.org/10.1016/j.cma.2024.117297>.
- [38] H. Li, T.Y. Zhong, G.H. Chen, D.X. Yang, Dynamic reliability-based robust design optimization for lead rubber bearings of girder bridges via direct probability integral method, *Struct Multidiscip Optim* 68 (2025) 198, <https://doi.org/10.1007/s00158-025-04099-4>.
- [39] Y. Zhang, M. Wiercigroch, G.H. Chen, D.X. Yang, Nonlinear stochastic dynamics of NES-based energy harvesters under random excitation via DPIM, *Mech Syst Signal Process* 241 (2025) 113507, <https://doi.org/10.1016/j.ymssp.2025.113507>.
- [40] Liu JR, Yang DX, Dang C, Valdebenito MA, Faes MGR. A single-loop reweighted numerical integration method for failure probability function estimation under parametric probability boxes (under review) 2025. <https://doi.org/10.2139/ssrn.5549566>.
- [41] J.B. Chen, J.Y. Yang, J. Li, A GF-discrepancy for point selection in stochastic seismic response analysis of structures with uncertain parameters, *Struct Saf* 59 (2016) 20–31, <https://doi.org/10.1016/j.strusafe.2015.11.001>.
- [42] J.R. Liu, X. Chen, G.H. Chen, R. Li, D.X. Yang, Exact benchmark solutions of stochastic responses and reliabilities of structures via the probability density integral equation, *ASCE-ASME J Risk Uncertain Eng Syst Part Civ Eng* 12 (2026) 04025086, <https://doi.org/10.1061/AJRUA6.UENG-1718>.
- [43] D.O. Loftsgaarden, C.P. Quesenberry, A Nonparametric Estimate of a Multivariate Density Function, *Ann Math Stat* 36 (1965) 1049–1051, <https://doi.org/10.1214/aoms/1177700079>.
- [44] L. Devroye, L. Györfi, G. Lugosi, *A Probabilistic Theory of Pattern Recognition*, Springer, New York, NY, 1996, <https://doi.org/10.1007/978-1-4612-0711-5>.
- [45] L. Ceriani, P. Verme, The origins of the Gini index: extracts from *Variabilità e mutabilità* (1912) by Corrado Gini, *J Econ Inequal* 10 (2012) 421–443, <https://doi.org/10.1007/s10888-011-9188-x>.
- [46] C.T. Zhong, G. Li, Z. Meng, H.J. Li, A.R. Yildiz, S. Mirjalili, Starfish optimization algorithm (SFOA): a bio-inspired metaheuristic algorithm for global optimization compared with 100 optimizers, *Neural Comput Appl* 37 (2025) 3641–3683, <https://doi.org/10.1007/s00521-024-10694-1>.
- [47] C. Dang, P.F. Wei, J.W. Song, M. Beer, Estimation of failure probability function under imprecise probabilities by active learning-augmented probabilistic integration, *ASCE-ASME J Risk Uncertain Eng Syst Part Civ Eng* 7 (2021) 04021054, <https://doi.org/10.1061/AJRUA6.0001179>.
- [48] C. Sun, V. Jahangiri, Bi-directional vibration control of offshore wind turbines using a 3D pendulum tuned mass damper, *Mech Syst Signal Process* 105 (2018) 338–360, <https://doi.org/10.1016/j.ymssp.2017.12.011>.